JMEPEG (2009) 18:679–685
DOI: 10.1007/s11665-009-9361-6

1059-9495/$19.00

Stress-Induced Martensitic Transformation in the Crack Tip Region of a NiTi Alloy

A. Falvo, F. Furgiuele, A. Leonardi, and C. Maletta

(Submitted September 23, 2008)

The evolution of stress-induced martensitic transformation in front of the crack tip in a NiTi alloy is analyzed in this investigation, by two-dimensional finite element simulations of single edge-crack specimens. In particular, the transformation start and finish contours, i.e., the boundaries of the transformation zone, were obtained by using plasticity concepts, and the effects of the temperature were taken into account by using the Clausius-Clapeyron relation. Furthermore, comparisons between numerical and analytical results, obtained by Irwin's modified linear elastic fracture mechanics relations, were carried out. These comparisons show that a good agreement in terms of the martensite start and finish sizes is obtained; moreover, the analytic approach could be able to describe the stress field in the crack tip region outside the phase transformation zone, i.e., in the austenitic region, but a proper equation to estimate the effective crack length should be found. To this aim, further studies should be carried out.

Keywords cracks, finite element analyses, fracture, NiTi alloys, shape memory alloys, stress-induced martensitic transformation

1. Introduction

In the last decades, shape memory alloys (SMAs), and in particular the Nickel Titanium-based ones (NiTi), have received more attention from scientific and engineering communities, owing to their unique characteristics, namely shape memory effect (SME) and superelastic effect (SE) (Ref 1). In particular, these properties allow large recoverable strains or large induced internal forces due to a reversible solid-state phase transformation between austenite and martensite; this transformation can be activated by a temperature variation (TIM, thermally induced martensite) or by the application of external forces (SIM, stress-induced martensite). Due to these interesting features, as well as to their good mechanical performances and biocompatibility, NiTi alloys have seen growing use in the last years in many branches of engineering and medicine. As a direct consequence of this interest, many researchers have studied the thermo-mechanical behavior of SMAs, in terms of both SME and SE (Ref 1), and various numerical models have been developed in order to describe their mechanical and functional behavior (Ref 2). However, a limited number of works have been devoted to the study of the fatigue (Ref 3-6) and, above all, fracture behavior (Ref 7-11) of NiTi alloys. From a materials science point of view, an accurate knowledge of these topics is essential for predicting the functional and structural life of damaged structures as well as their failure modes, with the aim to improve the overall performances of NiTi-based components or structures. The fracture behavior of austenitic NiTi alloys strongly depends on the SIM transformation which occurs in the crack tip region, as a consequence of the high values of local stresses.

In an experimental investigation of fracture mechanics in NiTi alloys (Ref 11), it has been shown that the crack is stress control propagated in line with the direction of the maximum normal stress. In addition, it was observed that the notch geometries and the martensitic transformation play significant roles on the fracture process of SMAs. In the last years, some finite element analyses concerning the martensitic transformation in front of notches or cracks have been carried out (Ref 12, 13); in particular, it has been found that the shape of the martensitic transformation zone at the crack tip is similar to the characteristic shape of plastic zone for metals. This means that modified plasticity concepts can be used to predict the transformation zone in SMAs.

In the present work, two-dimensional (2D) numerical simulations were carried out in order to investigate the effects of the temperature on the stress-strain distributions and on the martensitic transformation zone in front of the crack tip in a single edge-crack (SEC) specimen. Furthermore, comparisons between numerical and analytical results, obtained by Irwin's modified linear elastic fracture mechanics relations, were carried out. These comparisons show that a good agreement in terms of the martensite start and finish sizes is obtained; moreover, the analytic approach could be able to describe the stress field in the crack tip region outside the phase transformation zone, i.e., in the austenitic region, but a proper equation to estimate the effective crack length should be found. To this aim, further studies should be carried out.

This article is an invited paper selected from presentations at Shape Memory and Superelastic Technologies 2008, held September 21-25, 2008, in Stressa, Italy, and has been expanded from the original presentation.

A. Falvo, F. Furgiuele, A. Leonardi, and **C. Maletta**, Department of Mechanical Engineering, University of Calabria, 87036, Arcavacata di Rende, Italy. Contact e-mail: carmine.maletta@unical.it.

2. Constitutive Behavior

The classic simplified isothermal stress-strain curve for an austenitic NiTi-based SMA is represented with the solid piecewise line in Fig. 1. It is worth noting that this curve is relative to a monotonically increasing loading path, while if the load is decreased before failure the material exhibits the typical stress-strain hysteretic behavior, as the unloading path is represented by the dashed lines in Fig. 1. In the figure, the stress-strain relation is approximated with a piecewise linear curve, for sake of simplicity. The figure clearly shows that, when the applied load is increased, the SIM transformation (A $\rightarrow$ M) starts as σ reaches a critical value σ_s^{AM}, and the transformation is completed when σ is equal to σ_f^{AM}, i.e., the martensite fraction ξ_M increases from 0 to 1 and the material exhibits a characteristic deformation namely, ε_L. When unloading, the reverse transformation (M $\rightarrow$ A) occurs in the stress range σ_s^{MA}-σ_f^{MA}, resulting in a stress-strain hysteretic behavior. However, unloading and the corresponding reverse transformation (martensite to austenite) are not taken into account in this investigation since, for fracture purposes, the specimens for toughness measurements are generally loaded to fracture without unloading.

The main thermo-mechanical properties of the material, to be used in the numerical model described in the following section, were experimentally obtained in a previous work of the authors (Ref 14) by carrying out different isothermal tensile tests on dog bone-shaped test specimens in Ni-49 at.% Ti sheet (Type S, Memory Metalle, Germany, 0.75 mm thick) with a nominal austenite finish temperature $A_f = -7$ °C, as shown in Fig. 2.

The test were executed by using a universal testing machine (Instron 8500), equipped with a furnace (MTS 653) and a resistance extensometer with a gauge length of 10 mm. The stress-strain hysteretic behavior of the material was measured by isothermal strain controlled cycles, at a strain rate of 200 $\mu\varepsilon$ s^{-1}, that were carried out for different values of maximum deformation and at different temperatures. Figure 3(a) shows the evolution of the stress-strain hysteretic behavior of the material in the first 25 mechanical cycles for a fixed value of total strain $\varepsilon_{tot} = 3.5\%$. As well known (Ref 1, 14), the figure clearly shows that the material exhibits a strong modification of the stress-strain response in the first cycles, but the stress-strain loops become stable after 20 cycles and no significant modifications are observed with further increasing the number of mechanical cycles.

Figure 3(b) shows the modification of the isothermal stress-strain hysteresis loops under different values of the temperature for $T > A_f$, in the temperature range between 303 K and 328 K.

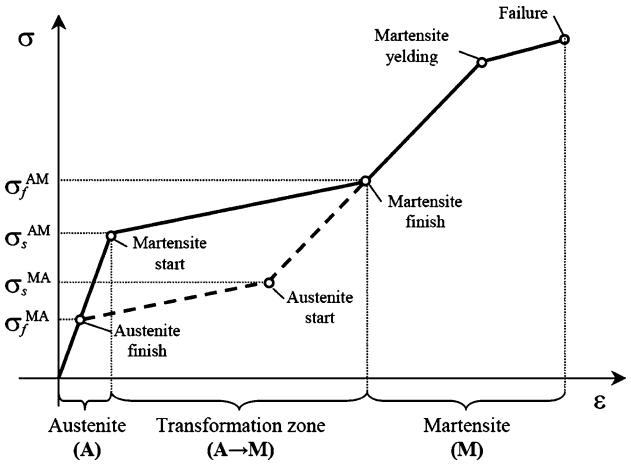

Fig. 1 Typical stress-strain relation of an austenitic NiTi alloy

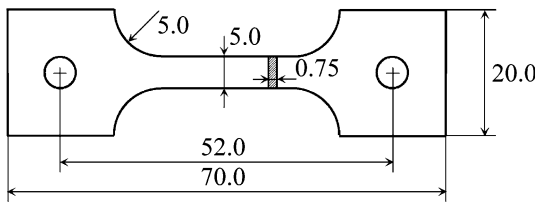

Fig. 2 Test specimen

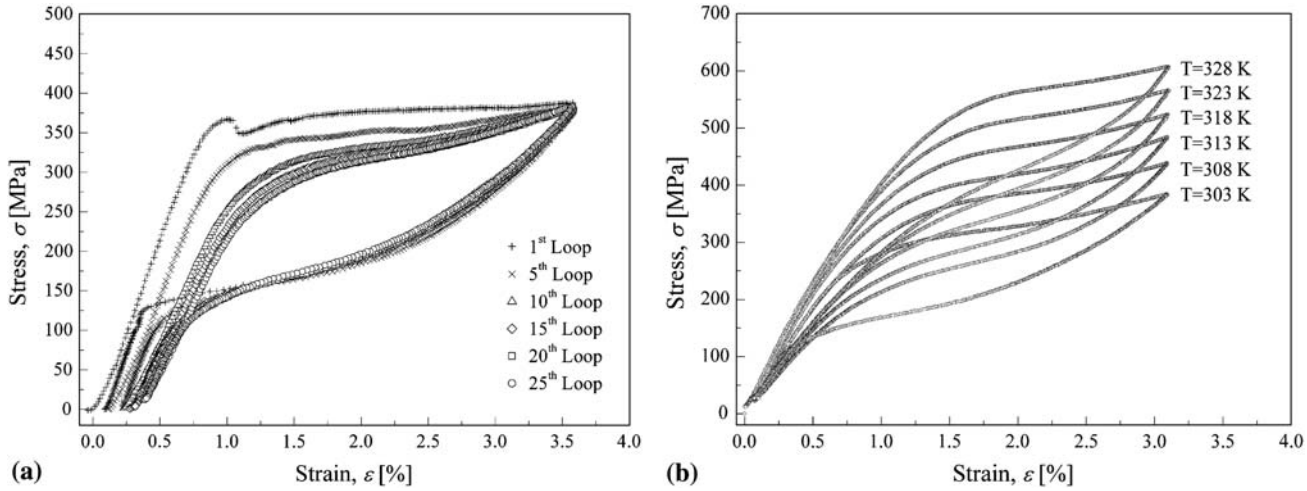

Fig. 3 Isothermal stress-strain hysteretic behavior: (a) evolution in the first 25 cycles at $T = 303$ K; (b) for different values of the temperature (303-328 K)

These results were used to measure the constants of the Clausius-Clapeyron relation:

$$\frac{d\sigma}{dT} = \text{const.} \quad \text{(Eq 1)}$$

which define the change in the stress for the onset of martensite during loading and the stress to obtain austenite during unloading.

Let C^{AM} be the constant governing the austenite-to-martensite transformation, then the critical stress values can be obtained as follows:

$$\begin{cases} \sigma_s^{AM} = \sigma_{s0}^{AM} + C^{AM}(T - T_0) \\ \sigma_f^{AM} = \sigma_{f0}^{AM} + C^{AM}(T - T_0) \end{cases}, \quad \text{(Eq 2)}$$

in which the subscript 0 is referred to the quantities measured at the reference temperature (T_0 = 303 K). In Table 1, the values of C^{AM}, σ_{s0}^{AM}, and σ_{f0}^{AM} for the investigated NiTi alloy, together with the Young's moduli and the Poisson's ratios, are reported.

3. Numerical Model

A SEC specimen was analyzed by 2D plane stress FE analyses carried out with the commercial finite element code MSC Marc®. The geometry and the dimensions of the SEC specimen are illustrated in Fig. 4, while Fig. 5 shows the corresponding FE model.

Due to the symmetry of the SEC specimen, only the upper half of the whole specimen was modeled. The model consists of 5629 eight-node bi-quadratic plane stress quadrilateral elements. A nonuniform mesh was introduced by employing a relatively fine mesh in the crack tip region, and a coarse mesh elsewhere, as clearly shown in Fig. 5.

The tensile load is applied on the upper half of the hole. As previously explained, unloading and the corresponding reverse transformation processes, from martensite to austenite (M → A), are not taken into account.

The isothermal stress-strain curves of the NiTi alloy, used in the numerical model, have been obtained for any temperature from data in Table 1, and by applying Eq 2; the resulting piecewise linear-stress relations are shown in Fig. 6, in which ε_L was fixed to 7%. Furthermore, the curves in Fig. 6 were truncated at a maximum stress equal to 1000 MPa, i.e., the yielding of martensite was not modeled, as the size of the transformation zone in the crack tip region is expected to be much greater than the plastic zone of the martensitic structure.

The martensite volume fraction, ξ_M, during the SIM, can be described by the equivalent plastic strain ε_{eq}^p (Ref 13). Indeed, the yielding condition for a conventional material is:

$$\sigma_{eq} = Y_p\left(\varepsilon_{eq}^p\right), \quad \text{(Eq 3)}$$

while the phase transformation condition in a SMA is:

$$\sigma_{eq} = Y_M(\xi_M), \quad \text{(Eq 4)}$$

in which σ_{eq} is the von Mises equivalent stress, while Y_p and Y_M are the plastic and transformation hardening function, respectively. By comparing Eqs 3 and 4, it emerges that the

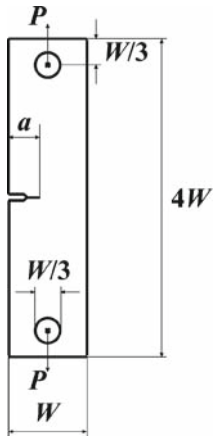

Dimensions [mm]	
Width, W	17,60
Crack length, a	6,80
Thickness, t	1,00

Fig. 4 SEC specimen geometry and dimensions

Table 1 Thermo-mechanical parameters of a Ni-49 at.% Ti alloy

E_A, MPa	ν_A	E_M, MPa	ν_M	σ_{s0}^{AM}, MPa	σ_{f0}^{AM}, MPa	C^{AM}, MPa K^{-1}
39000	0.3	20000	0.3	260	618.4	10.3

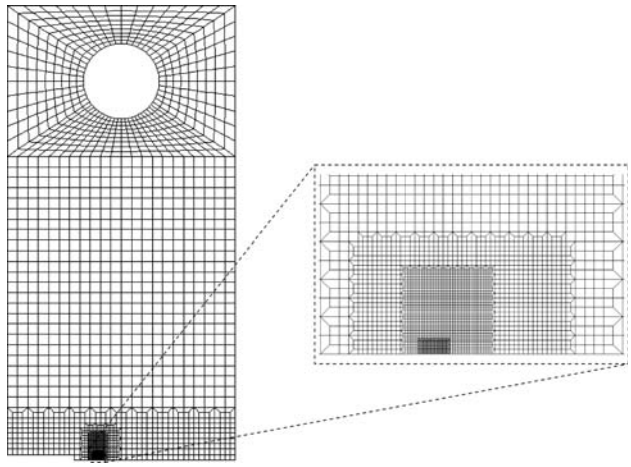

Fig. 5 FE model of the SEC specimen

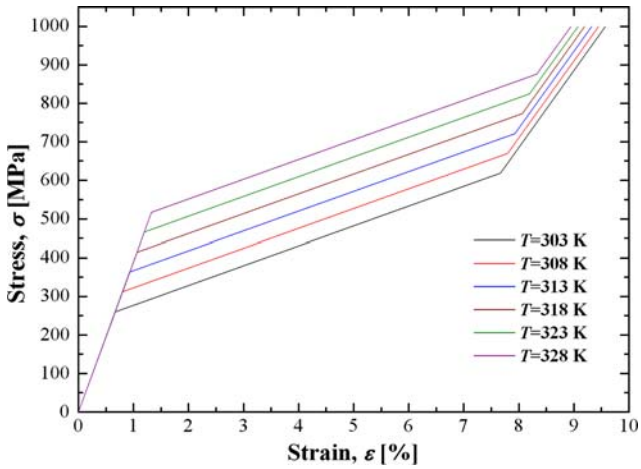

Fig. 6 Piecewise linear stress-strain relation of the NiTi alloy at several temperatures

transformation condition in SMAs is similar to the plastic yield condition in common metals, thus a simple linear relation between ξ_M and ε_{eq}^p can be assumed (Ref 15):

$$\xi_M = C\varepsilon_{eq}^p, \quad \text{(Eq 5)}$$

where C is a constant, which can be easily obtained from the uniaxial stress-strain relation of the SMA. In fact, at the beginning of phase transformation, the martensitic fraction and the equivalent plastic strain are zero, while at its end the martensitic fraction is 1 and the equivalent plastic strain is given by:

$$\varepsilon_{eq}^p = \varepsilon_{eq} - \varepsilon_{eq}^{el} = \varepsilon_{eq} - \frac{\sigma_{eq}}{E_A}, \quad \text{(Eq 6)}$$

in which ε_{eq} and ε_{eq}^{el} are the total and elastic equivalent strain, respectively. For the piecewise linear stress-strain relations used herein, ε_L and C^{AM} are constant, thus the equivalent plastic strain value at the end of the transformation is also constant and equals to 6.08×10^{-2}. By substituting these values into Eq 5, it follows:

$$C = \frac{\xi_M}{\varepsilon_{eq}^p} = \frac{1}{6.08 \times 10^{-2}} \approx 16.44. \quad \text{(Eq 7)}$$

Therefore, the distributions of martensite volume fraction ξ_M in front of the crack tip can be obtained by the distributions of the equivalent plastic strain ε_e^p through the following equation:

$$\xi_M = 16.44\varepsilon_{eq}^p. \quad \text{(Eq 8)}$$

4. Analytical Model

As it is well known, the normal stress σ_y, for $\theta = 0$, given by the linear elastic fracture mechanics (LEFMs) in the case of mode I loading condition is given by:

$$\sigma_y = \frac{K_I}{\sqrt{2\pi r}}, \quad \text{(Eq 9)}$$

in which r is the radial distance from the crack tip and K_I is the mode I stress intensity factor (SIF). For the SEC specimen in Fig. 4 (Ref 16), the SIF can be evaluated as follows:

$$K_I = \frac{P}{t\sqrt{W}}\sqrt{7.59\frac{a}{W} - 32\left(\frac{a}{W}\right)^2 + 117\left(\frac{a}{W}\right)^3}. \quad \text{(Eq 10)}$$

Equation 9 shows that the elastic stress would become very large in the proximity of the crack tip, but it does not occur due to SIM, which causes a different stress distribution; a similar behavior is observed in ductile metals due to the nonlinear effects of the plastic deformations. Irwin (Ref 17) has shown that when yielding occurs at the crack tip in common metals, LEFM may still be applied if an effective crack length is used, i.e., a physical crack length plus an allowance for the extent of the plastic zone:

$$a_{eff} = a + r_y. \quad \text{(Eq 11)}$$

where r_y can be expressed as a function of the size of the plastic zone r_p, as illustrated in Fig. 7; for plane stress conditions is given by:

$$r_y = \frac{r_p}{2} = \frac{1}{2\pi}\left(\frac{K_I}{S_y}\right)^2 \quad \text{(Eq 12)}$$

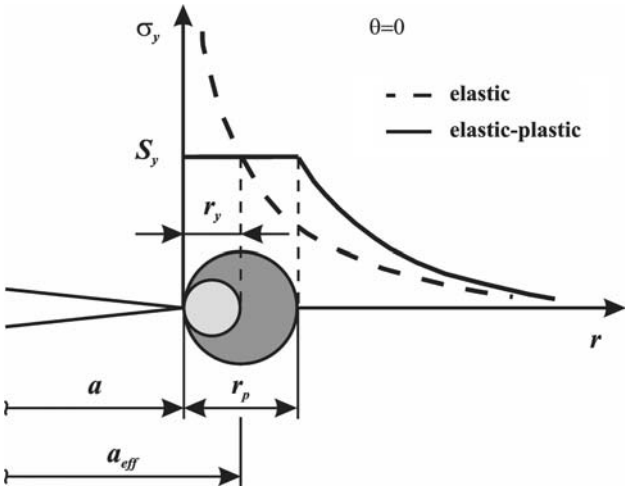

Fig. 7 Stress distribution in the crack tip region of a ductile metal

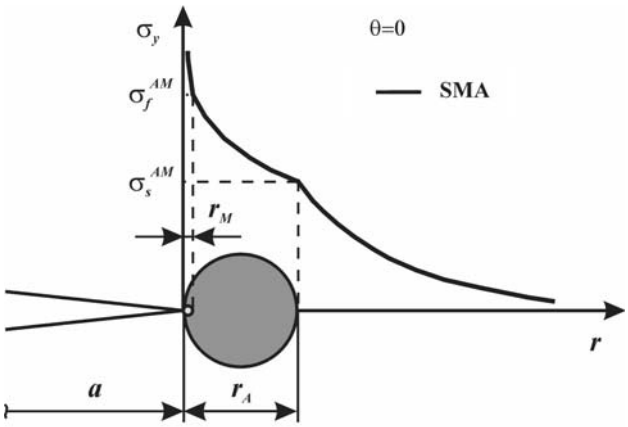

Fig. 8 Stress distribution in the crack tip region of an austenitic NiTi alloy

where S_y represents the yielding strength in ductile metals. Thus, the stress distribution in the crack tip region can be determined by the following equation:

$$\sigma_y = \frac{K_{Ieff}}{\sqrt{2\pi(r - r_y)}} \quad \text{(Eq 13)}$$

where K_{Ieff} is the effective SIF obtained by using $a_{eff} = a + r_y$ in Eq 10.

In Fig. 8, a schematic representation of the stress distribution in the crack tip region of an austenitic NiTi alloy is shown. The comparison between Fig. 7 and 8 shows that Eq 12 cannot be used to predict the size of the transformation zone, as a consequence of the different stress distributions in the crack tip region for ductile metals and NiTi alloys, since the equilibrium conditions are no more satisfied.

However, by assuming a linear evolution of the stress in the transformation zone, i.e., between σ_s^{AM} and σ_f^{AM}, and by neglecting the size of the martensitic zone, as $r_M \ll r_A$, the equilibrium condition can be rewritten as follows:

$$\frac{\sigma_s^{AM} + \sigma_f^{AM}}{2} r_A = \int_0^{r_A'} \sigma_y^{el} dr \quad \text{(Eq 14)}$$

where σ_y^{el} represents the stress distribution in the crack tip region of a linear elastic material (Eq 9), while r_A' is the extent of the transformation start contour, obtained by applying the condition $\sigma_y^{el} = \sigma_s^{AM}$:

$$r_A' = \frac{1}{2\pi}\left(\frac{K_I}{\sigma_s^{AM}}\right)^2 \quad \text{(Eq 15)}$$

By substituting Eq 9 in Eq 14 and taking into account Eq 15, the extent of the transformation start contour is given by:

$$r_A = \frac{2}{\pi}\frac{K_I^2}{\sigma_s^{AM}\left(\sigma_s^{AM} + \sigma_f^{AM}\right)}. \quad \text{(Eq 16)}$$

It is worth noting that in the case of elastic plastic material ($\sigma_s^{AM} = \sigma_f^{AM} = S_y$), the previous equation gives the extent of the plastic zone in common metals (Eq 12).

Based on the previous consideration, the Irwin correction can be applied to predict the stress distribution in the crack tip region of a NiTi alloy, by using the effective crack length:

$$a_{eff} = a + \frac{r_A}{2}. \quad \text{(Eq 17)}$$

Furthermore, Eq 13 gives the stress distribution in the crack tip region of a SMA by substituting $r_y = r_A/2$.

5. Results and Discussions

5.1 FE Model Validation

The FE model was initially validated by comparing the constitutive relation with the numerical results, in terms of the equivalent stress and strain ($\sigma_{eq} - \varepsilon_{eq}$), obtained in the crack tip region for a tensile load $P = 360$ N, which corresponds to a remote stress $\sigma^{\infty} = P/(tW) = 20.45$ MPa.

The comparisons between constitutive relation and numerical results were carried out for several values of the temperature, and a good agreement was observed in all cases, as illustrated in Fig. 9 which illustrates the results for $T = 303$ K.

Figure 10 illustrates stress contours for the transformation start ($\sigma_{eq} = \sigma_s^{AM}$) and the transformation finish ($\sigma_{eq} = \sigma_f^{AM}$) conditions, together with the maximum stress $\sigma_{eq} = 1000$ MPa (see Fig. 6); as expected, the figure clearly shows that the size of the transformation zone is much greater than the zone limited by the condition $\sigma_{eq} = 1000$ MPa.

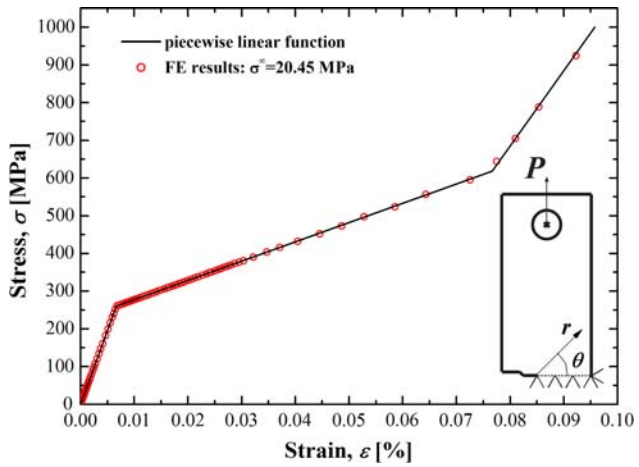

Fig. 9 Piecewise linear constitutive relation vs. FEM results ($T = 303$ K)

5.2 FE Results

By using Eq 8, the martensite volume fraction, ξ_M, in the crack tip region was computed for several values of the temperature in the range between 303 and 328 K; as an example, Fig. 11 shows the contours with constant ξ_M values at $T = 303$ K. The martensite volume fraction ξ_M in the partial martensite zone decreases with increasing the distance from the crack tip. Similar results have been obtained for all the investigated temperatures.

The transformation zone was analyzed by the distances from the crack tip and for $\theta = 0$ (see Fig. 9), which correspond to the transformation start (r_A) and finish (r_M) condition. In Fig. 12, the trends of r_A and r_M versus temperature are shown. The transformation start size rapidly decreases with increasing the temperature, while the transformation finish size is almost constant (it slightly decreases), resulting in an overall reduction of the transformation zone, which is represented by the gapping area between the curves in Fig. 12.

5.3 Analytical Predictions Versus Numerical Results

In Table 2, the numerical values of the martensite start region for different values of temperature are reported, together with the analytical predictions by LEFM and modified LEFM. The same results are schematically reported in Fig. 13.

The analytic approach underestimates the martensite start size for low values of the temperature while an overestimation is observed increasing the test temperature, giving relative differences of about 10%. These effects are due to the assumption $r_M \ll r_A$, taken to rewrite the equilibrium condition at the crack tip in the NiTi alloy, since the martensite finish radius, r_M, is not negligible respect to r_A with increasing the temperature, as shown in Fig. 12.

In Fig. 14, the numerical normal tension, σ_y, has been plotted versus the radial distance from the crack tip, r, for $T = 303$ K, in the stress-singularity region ($r < 2$ mm) in a bi-logarithmic plot. Increasing the distance from the crack tip, two knees are clearly visible, corresponding to the martensite finish and start, respectively; then, it is possible to identify in the graph the martensitic (M), the transformation (A $\rightarrow$ M) and the austenitic (A) regions. Using ordinary least square, the equation of the linear region of the austenitic zone was evaluated; in particular, the slope is -0.5, which corresponds to

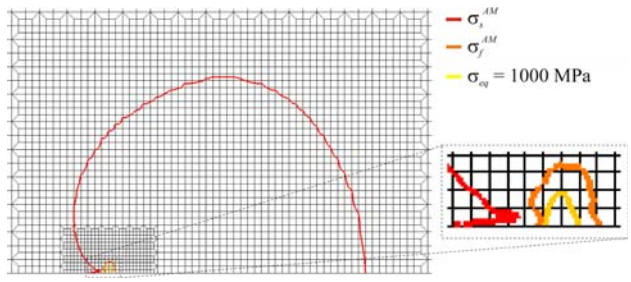

Fig. 10 Stress contours in the crack tip region: martensite start (*red*), martensite finish (*orange*) and $\sigma_{eq} = 1000$ MPa (*yellow*) ($T = 303$ K)

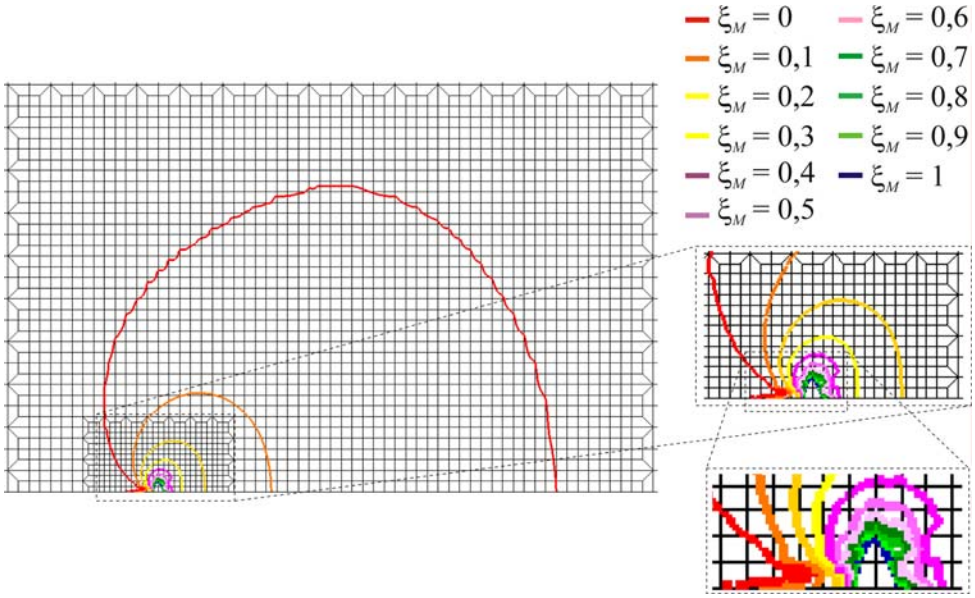

Fig. 11 Contour lines of constant martensite volume fraction ξ_M (T = 303 K)

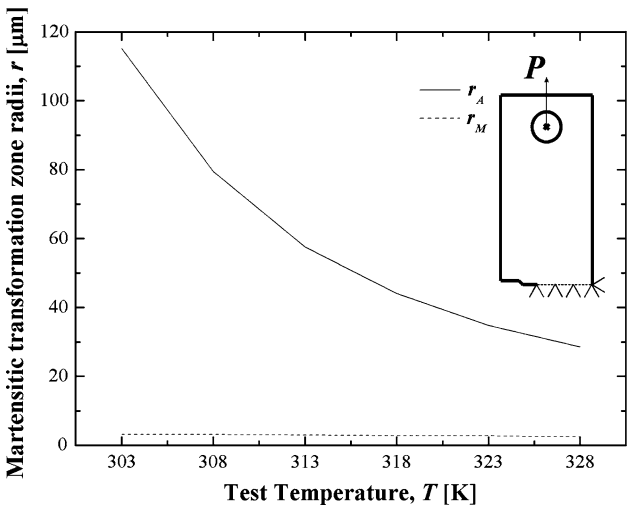

Fig. 12 Martensitic transformation zone vs. temperature, T

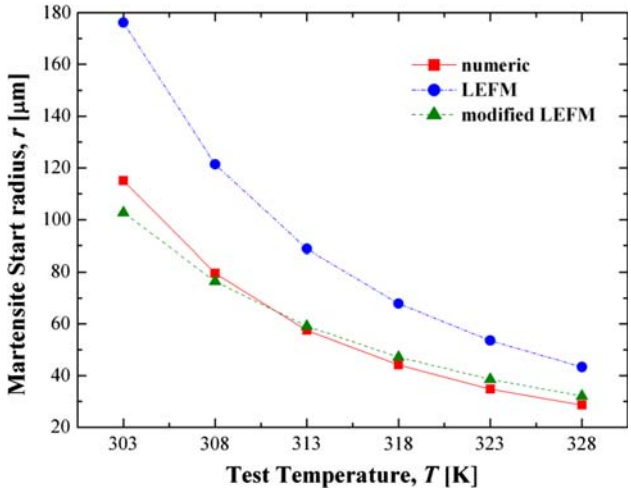

Fig. 13 Martensite start size, r_A, vs. temperature: LEFM, modified LEFM, and numerical results

Table 2 Martensite start size, r_A, for different temperatures: LEFM, modified LEFM, and numerical results

	r_A, μm		
T, K	LEFM	Modified LEFM	Numeric
303	176.2	102.8	115.1
308	121.4	76.4	79.5
313	88.8	59.1	57.5
318	67.8	47.1	44.1
323	53.5	38.5	34.8
328	43.3	32.1	28.6

the theoretical value of the LEFM. Thus, the Irwin correction (Eq 13) could be used to describe the stress distribution in a SMA for $r > r_A$, i.e., in the austenitic region, but not within the phase transformation zone.

In Fig. 15, a comparison between the numerical results and analytical predictions in terms of normal stress is presented for the reference temperature, T = 303 K. The figure shows similar trends between the curves; in particular, the LEFM overestimates the normal stress σ_y, while satisfactory agreement between the modified LEFM and numerical results has been obtained, with relative difference $<10\%$. Notwithstanding these differences, the results indicate that the modified Irwin correction of LEFM could be used to describe the stress distribution in the austenitic region but a proper equation should be found to estimate the effective crack length. In fact, the gap between the curves in Fig. 15 can be reduced by moving the vertical asymptote of the Irwin curve, i.e., by changing the value of r_y in Eq 13. Further studies should be carried out in order to define a modified relation for the effective crack length, which takes into account the whole stress-strain curve of the material, i.e., by considering the stress

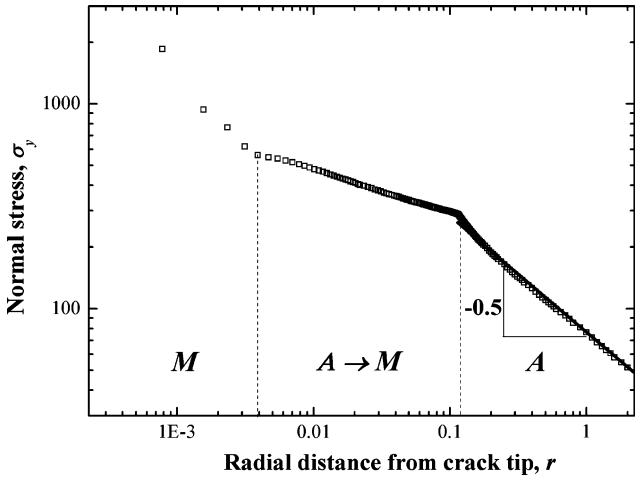

Fig. 14 Normal stress, σ_y, vs. radial distance from the crack tip, r (T = 303 K)

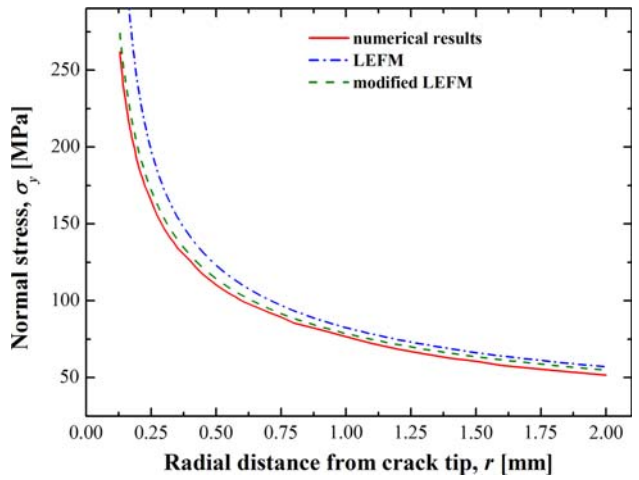

Fig. 15 Normal stress, σ_y, distribution in the austenitic region (T = 303 K)

distribution in the transformation zone as well as in the full martensitic region.

6. Conclusions and Perspectives

In the present work, the effects of the temperature on the stress-strain distributions and on the martensitic transformation zone in the crack tip region of a SEC specimen in NiTi alloy were analyzed by 2D numerical simulations. In particular, the martensite start and finish contours were evaluated from the numerical results. It was demonstrated that the distributions of martensite volume fraction, ξ_M, in front of the crack tip can be obtained by the distributions of the equivalent plastic strain. The numerical results, presented herein by contour lines, show that the martensite volume fraction ξ_M in the partial martensite zone gradually decreases with increasing the radial distance from the crack tip. Similar results have been obtained for all the investigated temperatures. Moreover, the numerical results show that the size of the transformation start rapidly decreases with increasing the temperature while the finish one is almost constant, resulting in an overall reduction of the transformation zone with increasing the temperature. Finally, comparisons between numerical and analytical results, obtained by Irwin's modified LEFMs relations, were carried out. These comparisons show that a satisfactory agreement in terms of the martensite start and finish sizes is obtained; moreover, the analytical approach could be able to describe the stress field in the crack tip region outside the phase transformation zone, i.e., in the austenitic region, but a proper equation to estimate the effective crack length should be found. To this aim, further studies should be carried out.

References

1. K. Otsuka and X. Ren, Physical Metallurgy of Ti-Ni-Based Shape Memory Alloys, *Prog. Mat. Sci.*, 2005, **50**, p 511–678
2. A. Paiva and M.A. Savi, An Overview of Constitutive for Shape Memory Alloys, *Math. Prob. Eng.*, 2006, **2006**, Art. no. 56876, p 1–30
3. G. Eggeler, E. Hornbogen, A. Yawnyl, A. Heckmann, and M. Wagner, Structural and Functional Fatigue of NiTi Shape Memory Alloys, *Mater. Sci. Eng. A*, 2004, **378**, p 24–33
4. M. Wagner, T. Sawaguchi, G. Kausträter, D. Höffken, and G. Eggeler, Structural Fatigue of Pseudoelastic NiTi Shape Memory Wires, *Mater. Sci. Eng. A*, 2004, **378**, p 105–109
5. G.B. Rao, J.Q. Wang, E.H. Han, and W. Ke, Study of Residual Stress Accumulation in TiNi Shape Memory Alloy During Fatigue Using EBSD Technique, *Mater. Lett.*, 2006, **60**, p 779–782
6. M. Guiomar de Azevedo Bahia, R. Fonseca Dias, and V. Tadeu Lopes Buono, The Influence of High Amplitude Cyclic Straining on the Behaviour of Superelastic NiTi, *Int. J. Fatig.*, 2006, **28**, p 1087–1091
7. S. Yi and S. Gao, Fracture Toughening Mechanism of Shape Memory Alloys due to Martensite Transformation, *Int. J. Solids Struct.*, 2000, **37**, p 5315–5327
8. S. Yi, S. Gao, and L. Shen, Fracture Toughening Mechanism of Shape Memory Alloys Under Mixed-Mode Loading due to Martensitic Transformation, *Int. J. Solids Struct.*, 2001, **38**, p 4463–4476
9. K. Gall, N. Yang, H. Sehitoglu, and Y.I. Chumlyakov, Fracture of Precipitated NiTi Shape Memory Alloys, *Int. J. Fract.*, 2001, **109**, p 189–207
10. G.M. Loughran, T.W. Shield, and P.H. Leo, Fracture of Shape Memory CuAlNi Single Crystals, *Int. J. Solids Struct.*, 2003, **40**, p 271–294
11. J.H. Chen, W. Sun, and G.Z. Wang, Investigation on the Fracture Behavior of Shape Memory Alloy NiTi, *Metall. Mater. Trans. A*, 2005, **36**, p 941–955
12. G.Z. Wang, Effects of Notch Geometry on Stress-Strain Distribution, Martensite Transformation and Fracture Behavior in Shape Memory Alloy NiTi, *Mat. Sci. Eng. A*, 2006, **434**, p 269–279
13. G.Z. Wang, A Finite Element Analysis of Evolution of Stress-Strain and Martensite Transformation in Front of a Notch in Shape Memory Alloy NiTi, *Mat. Sci. Eng. A*, 2007, **460-461**, p 383–391
14. C. Maletta, A. Falvo, F. Furgiuele, and J.N. Reddy, A Phenomenological Model for Superelasticity in NiTi Alloys, *Smart Mater. Struct.*, 2009, **18**, Art. no. 025005
15. Y. Jung, P. Papadopoulos, and R.O. Ritchie, Constitutive Modelling and Numerical Simulation of Multivariant Phase Transformation in Superelastic Shape-Memory Alloys, *Int. J. Numer. Meth. Eng.*, 2004, **60**, p 429–460
16. P.P. Milella, La MFLE nella pratica sperimentale, *Meccanica della Frattura Lineare Elastica ed Elastoplastica*, Chap. 4, Ansaldo Nucleare Editore, Ed., 1999, Italia, Genova (in italian)
17. G.R. Irwin, Plastic Zone Near a Crack and Fracture Toughness, *Proceedings of 7th Sagamore Ordnance Materials Conference*, 1960 (Syracuse, NY), Syracuse University Press, 1960, p 63–78